

MERIS Land Algorithm: Preliminary Validation Results

Nadine Gobron⁽¹⁾, Malcolm Taberner⁽¹⁾, Bernard Pinty⁽¹⁾,
Frédéric Mélin⁽²⁾, Michel M. Verstraete⁽¹⁾ and Jean-Luc Widlowski⁽¹⁾

(1) EC-JRC IES/GVM Unit, via E. Fermi 1, TP 440 I-21020 Ispra (VA), Italy, Email: nadine.gobron@jrc.it

(2) EC-JRC IES/IMW Unit, via E. Fermi 1, TP 272 I-21020 Ispra (VA), Italy

ABSTRACT

This paper presents a first and preliminary evaluation of the performance of the algorithm implemented in the Medium Resolution Imaging Spectrometer (MERIS) ground segment for assessing the status of land surfaces. First, we propose an updated version of the MERIS algorithm itself, which improves the accuracy of the product. Second, we analyze the first results by inter-comparing the MERIS Global Vegetation Index (MGVI) to similar products derived from the Sea-viewing Wide Field-of-view Sensor (SeaWiFS) that are generated at the European Commission Joint Research Center (EC-JRC). The first evaluation between MERIS and SeaWiFS derived products is made using data acquired on August 3, 2002 by both instruments. The results show acceptable agreement and the differences are well understood by radiation transfer models. Finally, we propose some recommendations to improve the current MGVI-land algorithm.

INTRODUCTION

Space remote sensing tools help monitor the characteristics of the landscapes and their temporal evolutions at a variety of spatial and temporal resolutions. The algorithms to retrieve surface properties from satellite data, in the optical domain, focus on the interpretation of the spectral signature of the various objects that interact with the solar radiation ultimately collected by a sensor. In particular, vegetation indices exploit the fact that green vegetation strongly absorbs (scatters) solar radiation in the red (near-infrared) spectral regions.

A generic approach to rationalize the design of spectral indices has been described in [11]. Using the physics of the signal and radiative transfer models, a first optimized algorithm for monitoring land surfaces has been developed for MERIS ([6] and [5]). The design of these generic algorithms is based on the following requirements: (1) they should exhibit a maximum sensitivity to the presence and changes in properties of healthy live green vegetation, and (2) they should not be sensitive to atmospheric scattering and absorption effects, to soil color and brightness changes and to temporal and spatial variations in the geometry of illumination and observation. Specific sensor algorithms must also be equivalent to each other in the sense of yielding the same biogeophysical information when applied to their respective data. These constraints imply that the land products should summarize the state of a given terrestrial system with a single number whose value must, by necessity, reflect only broad characteristics of the terrestrial ecosystems and their gross changes. The state and evolution of terrestrial ecosystems are characterized by a large number of physical, biochemical and physiological variables. The Fraction of Absorbed Photosynthetically Active Radiation (FAPAR) acts at once as an integrated indicator of the state of the plant canopy and can be retrieved by remote sensing techniques with acceptable accuracy. This has motivated the hypothesis that the FAPAR variable can be used to quantify the presence of vegetation with good reliability on a global scale, a variable of major importance for a variety of research and applied issues. Such a FAPAR/vegetation index has been developed for the SeaWiFS instrument and applied over multiple years of SeaWiFS data [2]. This SeaWiFS derived product thus provides a solid frame for investigating the quality of the corresponding MERIS FAPAR product.

After a short summary of the algorithm optimization, we discuss the potential improvements of the current version that can easily be incorporated into the MERIS processing chain. Finally, the inter-comparison between the two instrument products is presented and analyzed.

MGVI ALGORITHM

In a first step, we designed an extensive set of geophysical scenarios of sensor-like data sets representing various land surface conditions. This data set, used later on as a training data set for the algorithm, has been established on the basis of surface radiation transfer models coupled with atmospheric models. This approach yields a large number of simulated radiance fields, which can be sampled by a virtual instrument similar to the actual one in terms of the spectral and angular observation sampling schemes. The corresponding FAPAR values for the various simulated terrestrial

systems are simultaneously estimated as being part of radiation transfer model outputs. In the present case, simulations are conducted with a plane-parallel structurally homogeneous canopy model [4] for representing the land component; it is coupled with the 6S model [10] in order to represent the atmospheric effects. Since green vegetation strongly absorbs solar radiation in the red spectral region, and strongly scatters it in the near-infrared, these two bands are mostly used to characterize land surfaces from remote sensing data. The reflectance in the blue band is sensitive to the aerosol optical thickness and, therefore, is used to decontaminate the red and the near-infrared bands from atmospheric effects. The decontamination from directional effects is achieved using a parametric angular model.

The design of the FAPAR algorithm is based on a two step procedure where the spectral radiances measured in the red and near-infrared bands are, first, rectified in order to ensure their ‘decontamination’ from atmospheric and angular effects and, second, combined together in a mathematical formulae to generate the FAPAR value. The top of atmosphere (TOA) channel values are first “normalized” by the anisotropy function, to take into account the angular effects:

$$\tilde{\rho}(\lambda_i) = \frac{\rho^{toa}(\Omega_0, \Omega_v, \lambda_i)}{F(\Omega_0, \Omega_v, k_{\lambda_i}, \Omega_{\lambda_i}^{HG}, \rho_{\lambda_{ic}})}$$

Where λ_i stands for the wavelength (blue, red or near-infrared) of spectral band i , and $\rho^{toa}(\Omega_0, \Omega_v, \lambda_i)$ denotes the BRF values measured by the sensor in the spectral band λ_i , as a function of the actual geometry of illumination (Ω_0) and observation (Ω_v). These angular coordinates are fully defined by the zenith (θ) and relative azimuth (ϕ) angles for the incoming and outgoing radiation, respectively, for a plane-parallel system. The spectral anisotropy reflectance function, $F(\Omega_0, \Omega_v, k_{\lambda_i}, \Omega_{\lambda_i}^{HG}, \rho_{\lambda_{ic}})$, represents the shape of the radiance field. The triplet $(k_{\lambda_i}, \Omega_{\lambda_i}^{HG}, \rho_{\lambda_{ic}})$ are the RPV's parameters [9] either optimized *a priori* for each spectral band λ_i for mono angular instruments, or retrieved in the case of the multi-angular data, like with the Multi-angle Imaging Spectro-Radiometer (MISR) data [1].

The rectification process of the red and near-infrared bands is performed as follows:

$$\rho_{Rred} = g_1[\tilde{\rho}(\lambda_{blu}), \tilde{\rho}(\lambda_{red})] \quad \rho_{Rnir} = g_2[\tilde{\rho}(\lambda_{blu}), \tilde{\rho}(\lambda_{nir})]$$

$$\text{With } g_n(\rho_i, \rho_j) = \frac{l_{n1}\rho_i^2 + l_{n2}\rho_j^2 + l_{n3}\rho_i\rho_j + l_{n4}\rho_i + l_{n5}\rho_j + l_{n6}}{l_{n7}\rho_i^2 + l_{n8}\rho_j^2 + l_{n9}\rho_i\rho_j + l_{n10}\rho_i + l_{n11}\rho_j + l_{n12}}$$

The polynomial coefficients l_{nm} have been optimized in such a way that the values generated by each spectral

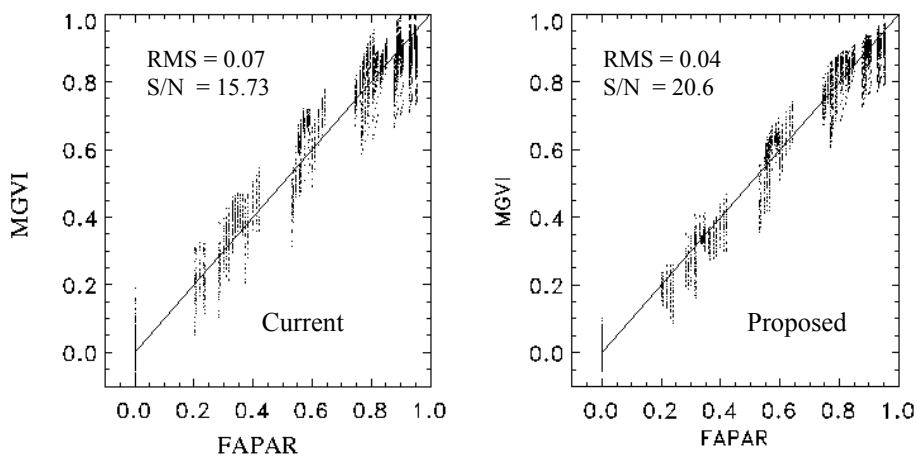


Fig. 1: Improvement of FAPAR accuracy from the updated training data set. The left panel corresponds to the current version of MGVI and the left panel to the proposed new version.

polynomial $g_n[\rho^{\sim}(\lambda_{bli}), \rho^{\sim}(\lambda_j)]$ correspond to the bi-directional reflectance factors that would be measured at the top of the canopy, normalized by the spectrally appropriate anisotropy reflectance function. In other words, the rectification process yields estimated values of spectral reflectance emerging at the top of the canopy, optimally decontaminated from atmospheric and angular radiative effects.

The FAPAR itself is then computed on the basis of these rectified channel values where the coefficients l_{0m} of polynomial g_0 have been optimized *a priori* to force $g_0(\rho_{Rred}, \rho_{Rnir})$ to take on values as close as possible to the FAPAR associated with the plant canopy scenarios used in the training data set.

Fig. 1 illustrates the improvement between the current algorithm (left panel) to the proposed new one (right panel) for which we obtain a smaller root mean square between the FAPAR and MGVI values and an increase of the signal over noise ratio from 15 to 20. The updated coefficients values for the new algorithm are summarized in tables 1 to 4.

Table 1. Optimal values of the parameters for the anisotropy function F

Channel λ_i (nm)	Parameter values		
	$\rho_{\lambda ic}$	$k_{\lambda i}$	$\Theta_{\lambda i}^{HG}$
442.5	0.24012	0.56192	-0.04203
681.25	-0.46273	0.70879	0.03700
865	0.63841	0.86523	-0.00123

Table 2. Optimal values of the coefficients for the polynomial g_1

$l_{11} = -9.2615$	$l_{12} = 3.2545$	$l_{13} = 9.8268$	$l_{14} = 0.537371$	$l_{15} = 0.363495$	$l_{16} = 0.00235486$
$l_{17} = 0.$	$l_{18} = 0.$	$l_{19} = 0.$	$l_{110} = 0.$	$l_{111} = 0.$	$l_{112} = 1.$

Table 3. Optimal values of the coefficients for the polynomial g_2

$l_{21} = -0.471310$	$l_{22} = -0.0451590$	$l_{23} = -0.807070$	$l_{24} = 0.198120$	$l_{25} = -0.00690978$	$l_{26} = -0.0210847$
$l_{27} = -0.0483620$	$l_{28} = -0.545070$	$l_{29} = -1.10270$	$l_{210} = 0.120625$	$l_{211} = 0.518928$	$l_{212} = -0.198726$

Table 4. Optimal values of the coefficients for the polynomial g_0

$l_{01} = 0.$	$l_{02} = 0.$	$l_{03} = 0.$	$l_{04} = -0.306$	$l_{05} = 0.255$	$l_{06} = 0.0045$
$l_{07} = 1.$	$l_{08} = 1.$	$l_{09} = 0.$	$l_{010} = 0.64$	$l_{011} = -0.64$	$l_{012} = 0.1998$

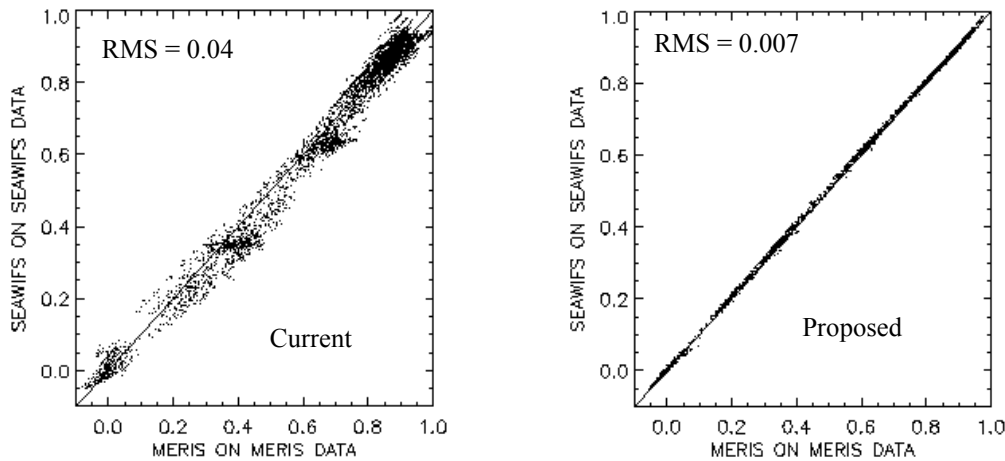


Fig. 2: Improvement of the algorithm accuracy. The comparison is made using simulated data for both the SeaWiFS and the MERIS sensors. The proposed algorithm increases dramatically the agreement between the estimations derived independently from both sensors.

Fig. 2 also shows the inter-comparison between FAPAR computed using the SeaWiFS algorithm with SeaWiFS simulated values against the corresponding MGVI/FAPAR values computed using the MERIS simulated scenarios. The right panel illustrates the better agreement between both sensor algorithms which basically translates into a reduction of the scatter of the points featuring the two FAPAR estimates

ACTUAL DATA INTER-COMPARISON

The proposed evaluation strategy consists in comparing the MGVI values to similar products derived from the SeaWiFS instrument on a single image acquired on August 3, 2002 by both instruments. This comparison requires first the re-mapping of the products from both instruments into the same geographical system [8]. In order to preserve the integrity of the MERIS level 2-land product, we have opted for a strategy of re-mapping the MERIS products into the SeaWiFS orbit.

The panels on Fig. 3 show the true-color maps for MERIS (left side) and SeaWiFS (right side) of the same geographical regions sampled within two hours difference by both MERIS and SeaWiFS on August 3, 2002. The extracted data set extends from the central of Europe to the South of Libya.

Since the time acquisition is not exactly the same, the atmospheric conditions and the relative geometries between both instruments are also different. The impact of these angular effects is partially corrected by the rectification procedure embedded in the FAPAR algorithm itself. However, the difference in relative azimuth angles between the sun and the instruments is rather large since SeaWiFS is pointing in the backward direction while MERIS is collecting measurements in the forward direction in this case. The impacts of these angular differences as well as the corresponding changes in atmospheric effects due to time difference of overpass have already been documented in a series of sensitivity studies [1] and [3].

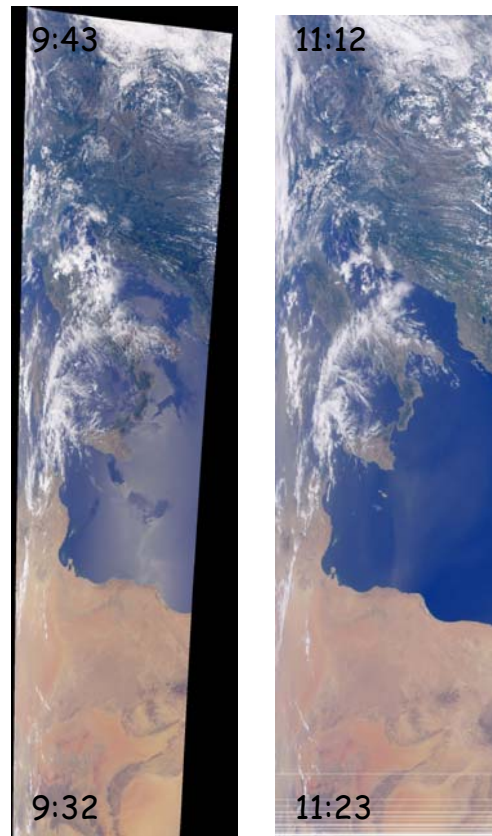


Fig. 3: Re-mapping the MERIS L1B data into the SeaWiFS orbit. The true-color maps of MERIS (left side) and SeaWiFS (right side) show the geographical domain sampled by both MERIS and SeaWiFS on August 3, 2002.

The differences in the relative geometry of illumination and observations existing for these two datasets are illustrated in Fig. 4. For the sake of explanation, all angle values are aggregated along track: the green line corresponds to the solar zenith angle, the purple line is for the view zenith angle and the red line represents the relative azimuth between the sun and the instrument. The effects on the FAPAR values delivered by the algorithms can be assessed first by the comparison on the two algorithms using simulated data with geometries close to the actual ones. The results are plotted on Fig. 5. It appears that, under these angular configurations, the SeaWiFS FAPAR values are slightly higher than those computed with MGVI, in particular for low to intermediate FAPAR values. This figure also illustrates the variability that may be expected due to the limitations inherent to the algorithm.

Finally, the comparison between the MERIS/MGVI and SeaWiFS/FAPAR values is summarized on Fig 6. Each value corresponds to a spatial average of 5 by 5 pixels to reduce possible problems due to the co-registration of pixels for both instruments during the re-mapping procedure. The left panel compares the aggregated values of MERIS/MGVI against the SeaWiFS/FAPAR showing a root mean square value equal to 0.08 and a bias close to 0.05. The bias is partly understood by the time difference in the data acquisition, as shown in Fig. 5, which is large enough to translate into actual FAPAR variations. The right panel illustrates the histogram of differences and it appears that 90 % of the pixels are inside the interval of difference of $[-0.1, +0.1]$, which is the anticipated daily accuracy of the products.

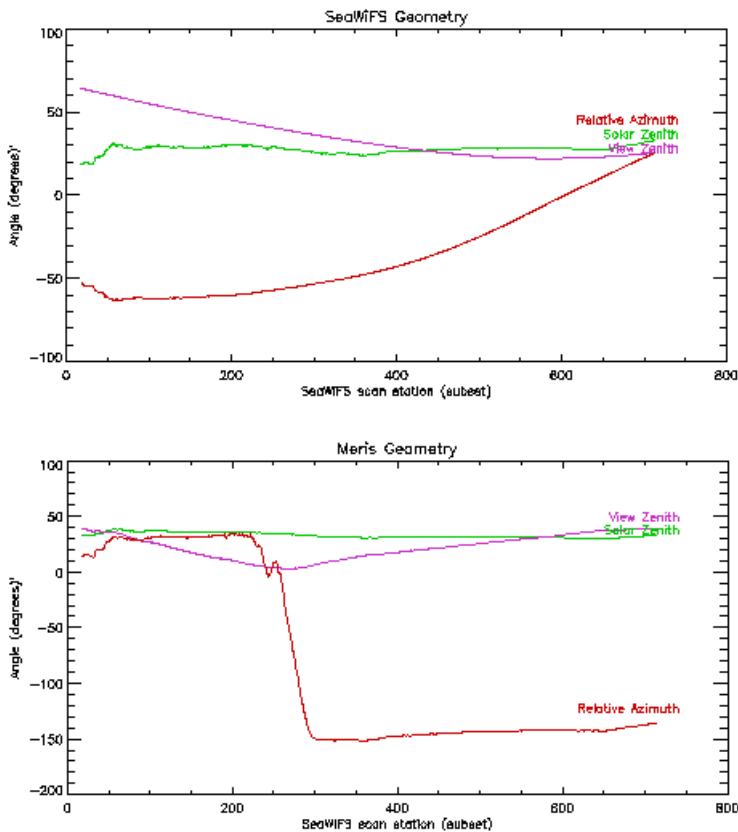


Fig. 4: Angular values aggregated along track for SeaWiFS (top panel) and MERIS (bottom panel) for the images acquired on August 3, 2002. The green line corresponds to the solar zenith angle, the purple line to the viewing zenith angle and the red line to the relative azimuth between the sun and the instrument.

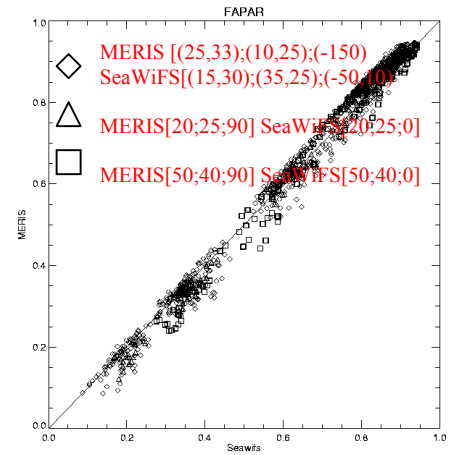


Fig. 5: Comparisons between the FAPAR values computed for both instruments with data measured in the same geometry of the actual data.

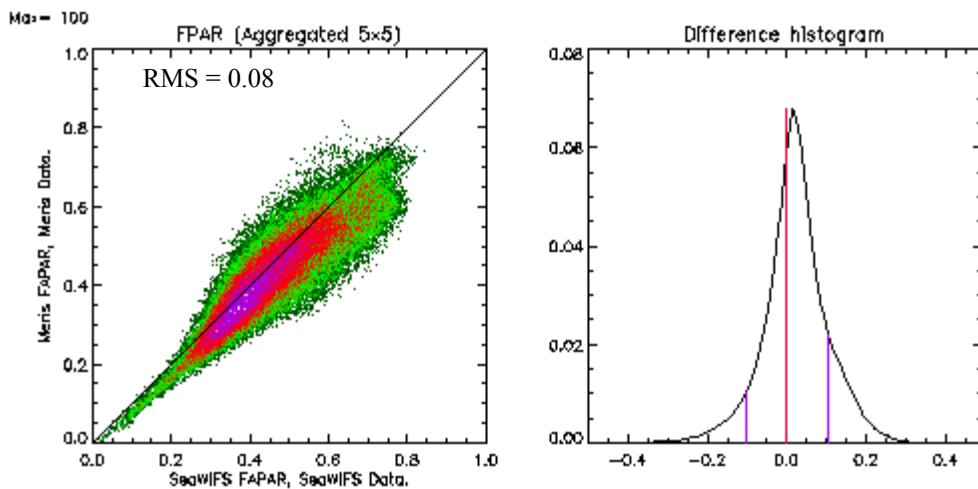


Fig. 6: Comparison between MGVI and SeaWiFS-Fapar averaged values of 5 by 5 pixels for the images acquired on August 3, 2002 (left panel) and histogram of difference between the two later values (right panel).

Fig 7. allows us to analyze the spatial consistency between both FAPAR maps as well as against an FAPAR reference map. The latter is a monthly composite map obtained for August 2000 with the SeaWiFS algorithm. The values correspond to the most representative values over the month following the composite technique described in [7]; it is therefore more likely to represent the most probable FAPAR field over that region and at this particular time of the year. For these three maps, the color scale of the FAPAR values varies from light white for low FAPAR value to red color for high FAPAR value. The white color pixels correspond to the clouds pixels, and the blue color identifies the water pixels.

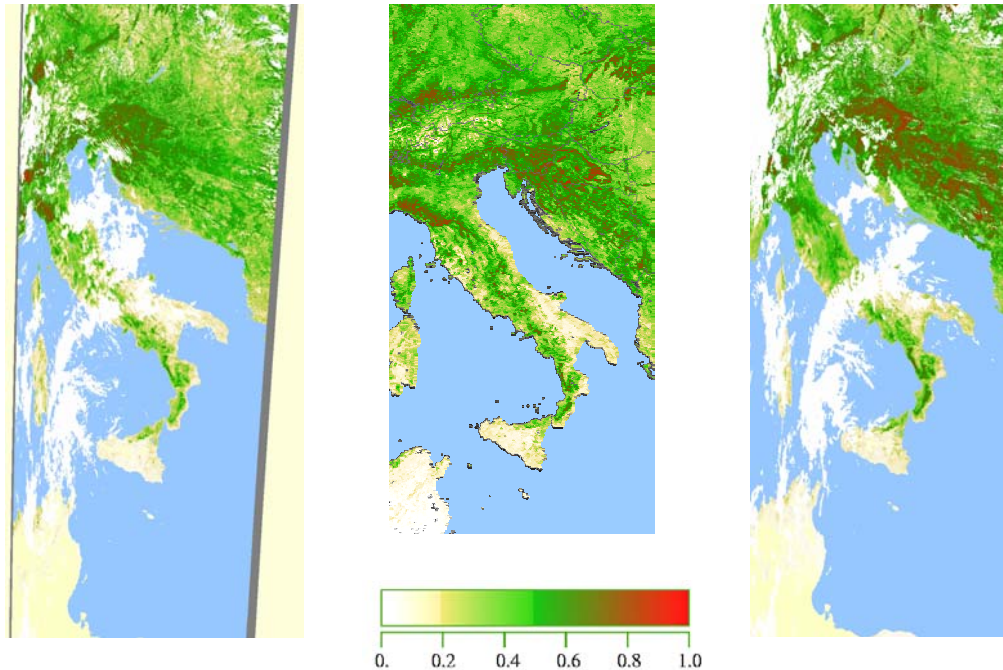


Fig. 7: FAPAR maps corresponding to 1) MERIS land product (left side) on the 3 August 2002, projected in the SeaWiFS orbit, 2) SeaWiFS (right side) on the 3 August 2002 and 3) August 2000 composite (middle) with SeaWiFS in a plate carrée projection.

PRELIMINARY CONCLUSIONS AND PERSPECTIVES

This paper presents preliminary results on the verification of the land product of the MERIS instrument, namely the MGVI, which aims at assessing the biophysical activities on land surfaces. Through the use of this algorithm the presence and health of live green vegetation over a wide diversity of terrestrial surfaces can be documented and monitored. The approach is based on a two step procedure: The first step aims at rectifying the red and near-infrared bands from the perturbing effects due to the atmosphere and the changes in the relative geometry of illumination and observation. The second step consists in optimizing the formula to approximate a one-to-one relationship between the index value and the Fraction of Absorbed Photosynthetically Active Radiation, used as a proxy for detecting the presence of healthy vegetation. The procedure capitalizes on the availability of advanced, coupled, surface-atmosphere radiation transfer models and uses them to construct the training data set against which the optimization is achieved for various instruments, including MERIS and SeaWiFS.

The updated version of the MGVI algorithm which has been derived for the MERIS sensor provides an improved accuracy for the estimation of the FAPAR values as well as an improved agreement between estimates made jointly by the MERIS and SeaWiFS sensors.

The preliminary validation of the proposed MGVI has been achieved by comparing the MGVI algorithm output against the corresponding SeaWiFS FAPAR product over a single scene. The results show acceptable agreement between the

two algorithms. The bias is well understood by radiation transfer model simulations and seems to be mainly due to the difference in the relative geometries. This contribution also illustrates the potential ability of the FAPAR to distinguish between various biome types, and their temporal dynamics. These geophysical products are well suited to address a number of issues related to the identification and monitoring of land surfaces. It is, however, proposed that the next round of improvement includes better identification between a series of geophysical conditions in order to facilitate future studies dealing with time and space composite. These identifiers could simply boil down to the implementation of additional flags from the level 1B.

ACKNOWLEDGEMENTS

The authors are grateful to Brockmann Consult (Geesthacht, Germany), ACRI (Sophia Antipolis, France) as well as ESA for continuing support during these preliminary validation activities. We would like to thank the SeaWiFS Project (Code 970.2) and the Distributed Active Archive Center (Code 902) at the Goddard Space Flight Center, Greenbelt, MD 20771, for the production and distribution of the SeaWiFS data, respectively.

REFERENCES

- [1] Gobron N., Pinty B., Verstraete M. M., Widlowski J.-L. and Diner D., 'Uniqueness of Multi-angular Measurements Part 2: Joint Retrieval of Vegetation and Photosynthetic Activity from MISR', *IEEE Transactions on Geoscience and Remote Sensing, MISR Special Issue*, **Vol. 40**, No 40, p 1574-1592, 2002.
- [2] Gobron N., Mélin F., Pinty B., Verstraete M. M., Widlowski J.-L. and Bucini, G. 'A Global Vegetation Index for SeaWiFS: Design and Applications', *Satellite Remote Sensing Data and Climate Model Simulations: Synergies and Limitations*, Edited by M. Beniston & M. M. Verstraete, Kluwer Academic Publishers, Dordrecht, 2001.
- [3] Gobron N., Pinty B., Verstraete M. M. and Widlowski J.-L., 'Advanced Spectral Algorithm and New Vegetation Indices Optimized for Up Coming Sensors: Development, Accuracy and Applications', *IEEE Transactions on Geoscience and Remote Sensing*, **Vol. 38**, No 6, p. 2489-2505, 2000.
- [4] Gobron N., Pinty B., Verstraete M. M. and Govaerts, Y., 'A semi-discrete model for the scattering of light by vegetation', *Journal of Geophysical Research*, **Vol. 102**, p. 9431-9446, 1997.
- [5] Gobron N., B. Pinty, M. M. Verstraete, and Y. Govaerts, 'The MERIS Global Vegetation Index (MGVI): Description and Preliminary Application', *International Journal of Remote Sensing*, **Vol. 20**, p. 1917-1927, 1999.
- [6] Govaerts Y., Verstraete M. M., Pinty B. and Gobron N., 'Designing an Optimal Spectral Index for Terrestrial Applications Based on MERIS Observations', *International Journal of Remote Sensing*, **Vol. 20**, p. 1853-1873, 1999.
- [7] Mélin F., Steinich C., Gobron N., Pinty B. and Verstraete M.M., 'Optimal Merging of LAC and GAC Data from SeaWiFS', *International Journal of Remote Sensing*, **Vol. 23**, No. 4, p 801-807, 2002.
- [8] Snyder J.P., 'Map projections used by the U.S. Geological Survey', *Geological Survey Bulletin*, 1532, 1982.
- [9] Rahman H., Pinty B., and Verstraete M.M., 'Coupled surface-atmosphere reflectance (CSAR) model. 2. Semi-empirical surface model usable with NOAA Advanced Very High Resolution Radiometer data', *Journal of Geophysical Research*, **Vol. 98**, 20,791-20,801, 1993
- [10] Vermote E., Tanré D., Deuze J.L., Herman M., and Morcrette J. J., 'Second simulation of the satellite signal in the solar spectrum: An Overview', *IEEE Transactions on Geoscience Remote Sensing*, **Vol. 35-3**, p. 675-686, 1998.

- [11] Verstraete M. M. and Pinty B., Designing optimal spectral indices for remote sensing applications, *IEEE Transactions on Geoscience and Remote Sensing*, **Vol. 34**, p. 1254-1265, 1996.